Geochemistry Geophysics Geosystems G3
AN ELECTRONIC JOURNAL OF THE EARTH SCIENCES
Published by AGU and the Geochemical Society

Article
Volume 9, Number 5
15 May 2008
Q05013, doi:10.1029/2007GC001744
ISSN: 1525-2027

Subdecadally resolved paleoceanography of the Peru margin during the last two millennia

Rajesh Agnihotri
School for Marine Science and Technology, University of Massachusetts Dartmouth, 706 South Rodney French Boulevard, New Bedford, Massachusetts 02744, USA

Now at National Institute of Oceanography, Dona Paula, Goa 403 004, India (rajagni9@gmail.com)

Mark A. Altabet
School for Marine Science and Technology, University of Massachusetts Dartmouth, 706 South Rodney French Boulevard, New Bedford, Massachusetts 02744, USA

Timothy D. Herbert and Jessica E. Tierney

Department of Geological Sciences, Brown University, Box 1846, Providence, Rhode Island 02912, USA

[1] Using multiproxy sediment core data from the El Niño–Southern Oscillation (ENSO)-sensitive Peru margin, subdecadally resolved (down to ~0.6 year) surface productivity and subsurface denitrification are reconstructed for the last ~2300 years. Scanning XRF generated major elemental data (Ti, Fe, Si) correlate well with discrete inductively coupled plasma-atomic emission spectometry (ICP-AES) analyses and together with X-radiography (core density) are used as productivity indices. As surface productivity in this marine region is strongly impacted by ENSO, higher (lower) periods of surface productivity are inferred to represent a persistent normal/La Niña (El Niño)-like state. Surface productivity and subsurface denitrification appear to have remained intimately coupled during this period due to direct stimulation of requisite subsurface suboxia and/or hydrographic restructuring. The late Holocene Peru margin is characterized by persistent moderate productivity and subsurface denitrification punctuated at centennial scale by shorter-duration periods of high production and intense denitrification. These centennial-scale events are likely analogous to modern observations of decadal-scale "regime shifts" but of higher amplitude and provide a background history for future natural changes to this system. Solar (irradiance) variability is suggested to have influenced Peru productivity as evidenced in numerous high-resolution paleorecords from the northern hemisphere.

Components: 6952 words, 9 figures.

Keywords: Peru margin; surface productivity; X-radiography; subsurface denitrification; solar forcing.

Index Terms: 1616 Global Change: Climate variability (1635, 3305, 3309, 4215, 4513); 1650 Global Change: Solar variability (7537); 4901 Paleoceanography: Abrupt/rapid climate change (1605).

Received 9 July 2007; **Revised** 13 February 2008; **Accepted** 12 March 2008; **Published** 15 May 2008.

Agnihotri, R., M. A. Altabet, T. D. Herbert, and J. E. Tierney (2008), Subdecadally resolved paleoceanography of the Peru margin during the last two millennia, *Geochem. Geophys. Geosyst.*, *9*, Q05013, doi:10.1029/2007GC001744.

1. Introduction

[2] Present-day controls of modern climate as well as the future course of anthropogenic climate change may be elucidated through identification of natural climate variability and dominant forcing(s) in the late Holocene before anthropogenic greenhouse effects became significant. Temporally well resolved Holocene records have been obtained from marine as well as continental repositories and numerous records from both low and high latitudes in the northern hemisphere show evidence for significant decadal- to centennial-scale climate oscillations, perhaps induced by solar irradiance forcing [*Agnihotri et al.*, 2002; *Fleitmann et al.*, 2003; *Gupta et al.*, 2003; *Wang et al.*, 2005; *Bond et al.*, 2001; *Hu et al.*, 2003; *Mangini et al.*, 2005]. However, relatively absent are comparable high-resolution paleorecords from the southern hemisphere, especially the tropics, leaving open the question of whether the observed Holocene climate variability was global in nature and if not, the nature of any phase lags between northern and southern hemispheres.

[3] The climate of the tropical Pacific and the Peru margin in particular is strongly impacted by the El Niño-Southern Oscillation (ENSO), the inter-annual weakening/strengthening of the equatorial Walker circulation that also remotely influences global climate through teleconnections [*Philander*, 1983; *Cane and Clement*, 1999]. The Peru margin is characterized by high surface biological activity driven by persistent coastal upwelling of nutrient rich waters from the poleward flowing subsurface (Peru) undercurrent. This undercurrent carries poorly ventilated waters of ultimately subantarctic origin promoting an intense subsurface oxygen minimum zone (OMZ) and substantial water column denitrification [*Liu*, 1979; *Codispoti et al.*, 1986; *Altabet*, 2005]. During El Niño conditions, relaxation of the Walker circulation causes warm, nutrient-poor surface waters of western equatorial Pacific origin to spread eastward ultimately suppressing isotherms and the oxycline along the Peru margin. Upwelling of nutrient-poor water causes reduction of primary productivity and crashes in fisheries [*Arntz and Fahrbach*, 1991]. ENSO has characteristic periodicities of 4 to 7 years [*Moy et al.*, 2002]. However, decadal-scale ENSO-like variability has also been noted in the eastern Pacific (Pacific decadal oscillation; PDO) [*Linsley et al.*, 2000].

[4] Excellent preservation of organic matter (OM) in rapidly depositing continental margin sediments underlying the OMZ off Peru permits high-fidelity preservation of proxy indicators of surface productivity (C_{org}, N, Opal contents, etc.) and subsurface denitrification (sedimentary $\delta^{15}N$) with minimal bioturbation influence. Therefore, high sedimentation rates (~mm/a) provide high-resolution paleoceanographic variability recorded in well-dated sediment cores from this region and thus an opportunity to characterize paleo-ENSO-like variability with respect to productivity and OMZ intensity beyond the inter-annual timescales observed in the modern period and assess likely forcings. Despite the paleoclimatic importance of this region, few high-resolution paleoceanographic reconstructions have been obtained from the Peru margin [*Rein et al.*, 2004, 2005]. This is attributed to (1) poor preservation of foraminiferal $CaCO_3$ limiting application of conventional dating schemes and (2) difficulty in achieving sufficient temporal resolution with conventional millimeter- to centimeter-scale sediment core sampling of sediment cores for proxy analysis.

[5] Recently, radiocarbon analysis of extracted sedimentary alkenones (exclusively produced from marine algal compounds) has been proven as a reliable dating tool in this region. By comparison with compound specific alkenone ^{14}C dates, *Higginson and Altabet* [2004] also demonstrated the validity of previously published ^{14}C dates of bulk organic carbon from the Peru margin [*Reimers and Suess*, 1983]. Hence, ^{14}C dating of bulk organic carbon yields reliable sediment core chronologies for this ENSO sensitive margin. A second important advancement has been the advent of scanning XRF determination of sediment core elemental composition at submillimeter scale with reasonable accuracy and precision [*Croudace et al.*, 2006]. Accordingly, very high temporal resolution records may be obtained, only limited by sediment accumulation rate and degree of bioturbation. The scanning XRF facility at Woods Hole Oceanographic Institute (WHOI) used in this study also provided X-radiographs (density) and optical imagery (sediment visual appearance) readily aligned with the chemical data.

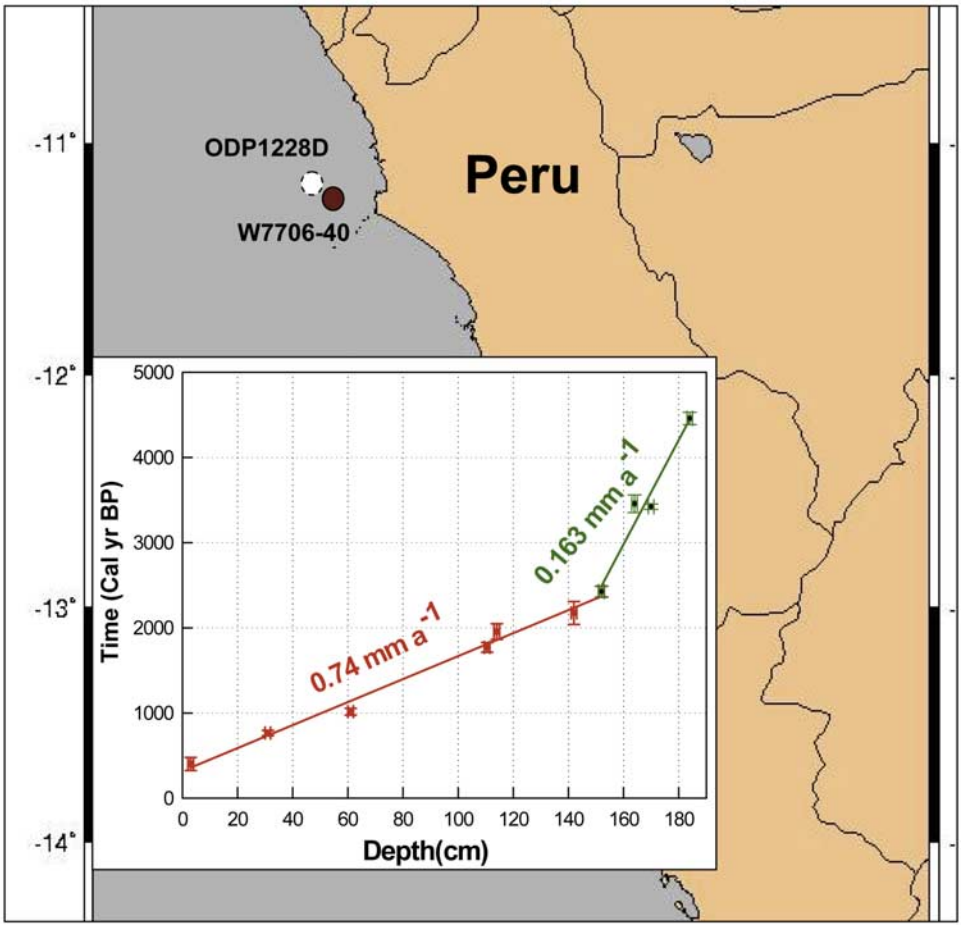

Figure 1. Location of core W7706–40 off Peru. Inset shows age-depth model used. Linear fit through initial seven ^{14}C dates shows linear sedimentation (~0.74 mm/a) for the last ~2300 years, before which sedimentation rate was sharply reduced (~0.16 mm/a). Vertical error bars represent 1σ uncertainty on calibrated ages and horizontal error bars show uncertainty on mean depths.

[6] Using these recent advances in sediment dating and high-resolution proxy detection, we have reconstructed the paleoceanographic history of the Peru margin spanning the last ~2300 years. Since ENSO is known to have a vital role in governing surface productivity off Peru on interannual timescales [*Arntz and Fahrbach*, 1991], we infer periods of increased surface productivity as representing a persistent normal or La Niña-like state with lower productivity periods as a persistent El Niño-like state. The ultrahigh-resolution major elemental data for Si, Fe and Ti generated by scanning XRF (at 0.04 cm depth intervals) is compared and calibrated with inductively coupled plasma-atomic emission spectometry (ICP-AES) measurements at cm-scale following conventional chemical digestion procedures. These data are compared to ultrahigh-resolution variations in sediment density determined by X-radiography. In addition, we also use bulk sedimentary N (wt. %) as an index of surface (organic) productivity and its isotopic ratio ($\delta^{15}N$) as an index of water column denitrification on the Peru margin, both measured at cm resolution.

2. Study Site

[7] The location of core W7706-40 (W40; 11.3°S 78.0°W, 186 m depth; Figure 1) lies on the edge of the Peruvian shelf within the region of high surface productivity and overlaid by suboxic waters that favor deposition of laminated organic-rich, diatomaceous sediments [*Kudrass*, 2000]. These suboxic waters experience substantial denitrification but not sulfate reduction [*Codispoti et al.*, 1986]. These waters are geographically found between ~5°S to 15°S, and contact the seafloor along the Peru margin between 150 and 400 m water depth [*Bruland et al.*, 2005]. During normal/La Niña conditions, intense coastal upwelling of cool, nutrient-rich waters fuels high surface productivity in the

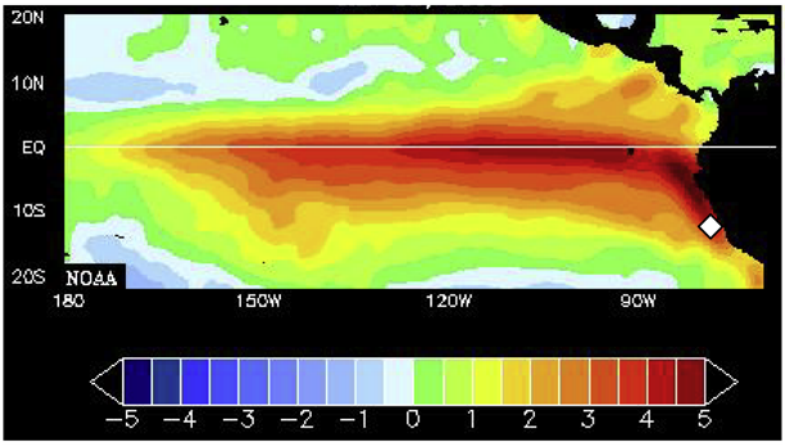

Figure 2. Sea surface temperature anomaly during the 1997/1998 El Niño (http://www.cdc.noaa.gov/map/clim/sst_olr/el_nino_anim.shtml) and core location of W40 off Peru.

region. During El Niño events, upwelling of nutrient rich water diminishes as the thermocline/nutricline deepens, resulting in warm surface water anomalies (Figure 2) and a substantial decrease in surface productivity, as observed by fishermen and modern instrumental data [*Arntz and Fahrbach*, 1991]. Both the reduced flux of carbon and depression of the thermocline moderate suboxic conditions along the Peru margin by corresponding deepening of the oxycline. Therefore, it is expected that a higher degree of water column denitrification would coincide with normal/La Niña conditions, while El Niño conditions should result in a suppression of subsurface denitrification on the Peru margin.

3. Methods

[8] The age-depth model of the core W40 (Figure 1 inset) was established using ^{14}C dating of bulk organic carbon. All radiocarbon ages were corrected assuming a reservoir age of 420 years and having 1σ error $\leq$ 150 years during the Holocene. Core W40 has a sedimentation rate of ~0.74 mm/a for the last ~2300 years before which sedimentation rate was significantly reduced (approximately 0.163 mm/a) (Figure 1 inset). We thus discuss in this report the paleoceanographic history spanning just the last ~2300 years due to the better temporal resolution and chronological constraints for this period in this core.

[9] Ultrahigh-resolution XRF data, optical and X-ray imageries were obtained at 0.4 mm depth intervals corresponding to an average temporal resolution of ~0.54 years. For other chemical and isotopic analysis, sediments were sampled every cm and freeze-dried prior to analysis. Measurements of N content (wt. %) and $\delta^{15}N$ were made on ~10–25 mg aliquots of homogenized dried bulk sediment. Bulk sedimentary $\delta^{15}N$ is considered equivalent to $\delta^{15}N$ of sedimentary OM, as inorganic nitrogen (NH_4^+) content is very small as compared to organic nitrogen in organic rich sediments [*Altabet et al.*, 1995, 1999]. Details of isotope analytical methods are published elsewhere [*Altabet et al.*, 1999]. All $\delta^{15}N$ data are relative to atmospheric N_2 and overall reproducibility of $\delta^{15}N$ measurements (including sample preparation and analyses) is better than ±0.2‰. The ultrahigh-resolution major element data measured by scanning XRF were calibrated/compared with discrete cm-scale chemical data. For these, admixtures of sediments samples (~0.4 g) and lithium metaborate (~0.16 g) flux were fused at ~1100°C in a furnace making a glass-bead which was dissolved in 10% HCl. Elemental concentrations were then determined using ICP-AES (JY-Horiba; facility at Brown University). Accuracy and analytical precision were checked using standard reference materials, which were better than 5% for all the major elements. The calibrations necessary to convert raw scanning XRF data to sediment concentration data were derived using results from nearby sediment core ODP1228D (Figure 1) for which both XRF and ICP-AES elemental data were available over a 0 to 3 mbsf core depth interval. We fully expect this calibration to apply to W40 given very the similar sediment compositions for each. Statistically significant correlations for the major elements Fe, Ti

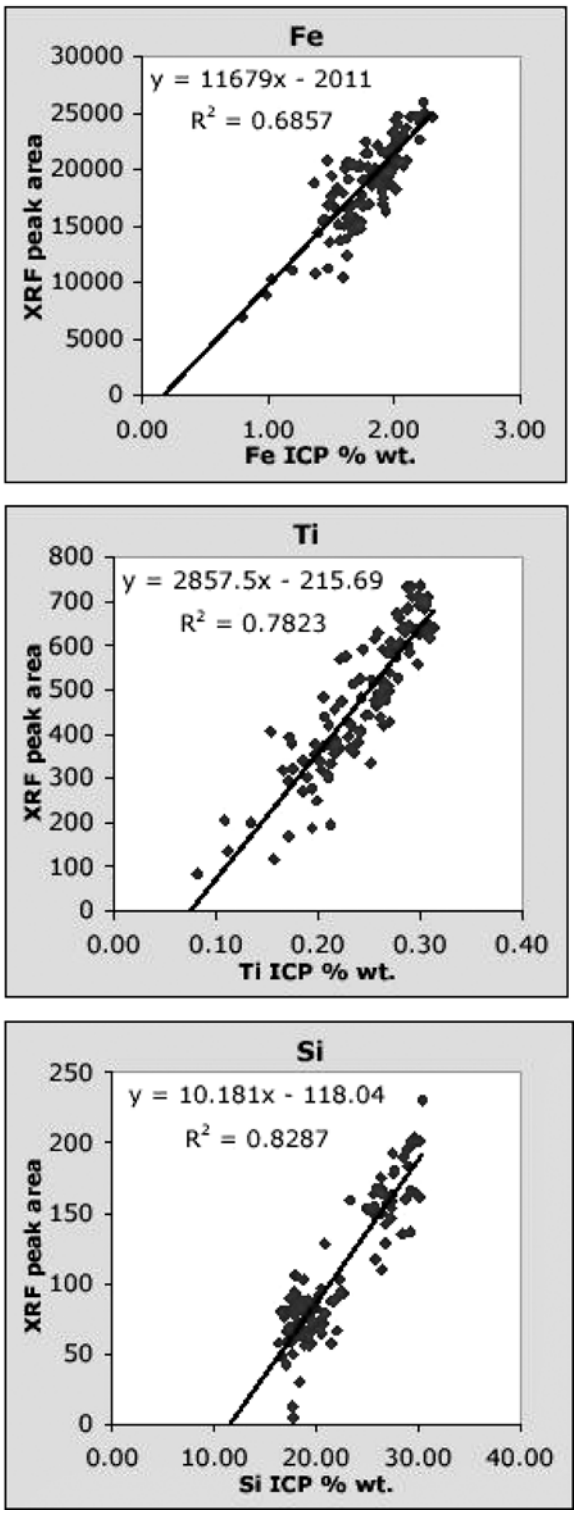

Figure 3. Calibration plots of major elements Fe, Ti, and Si measured by scanning XRF and ICP-AES for core ODP1228D.

and Si validate this approach (Figure 3). Since XRF data for discrete, homogenized samples show little scatter with respect to accepted values (not shown), some fraction of the scatter in the comparison of XRF data to conventional measurements are due to sediment inhomogeneities. Using these calibrations, ultrahigh-resolution XRF data for core W40 were converted to respective elemental concentrations and compared with concentrations measured at cm-scale by ICP-AES (every fifth depth interval). Fe, Ti and Si contents of core W40 measured by the two different techniques (Figure 4) also show statistically significant matches further validating the use of ultrahigh-resolution XRF data for paleoreconstruction in this region.

4. Results and Discussion

4.1. Surface Productivity Indices

[10] Optical and X-ray images of core W40 clearly reveal the presence of banding and periodic finer laminations throughout the core (Figure 5). X-ray images of the core were digitized to a gray scale index of 0 (Black) to 255 (white) using MATLAB (Figure 5). This gray scale index represents density variations in sedimentary material due to varying proportions of low-density biogenic (lighter) and higher-density continental lithogenic (denser/darker) components. Lighter X-radiograph gray scale indicates a higher proportion of biogenic components (e.g., biogenic opal and OM) and likely higher surface productivity, whereas darker gray scale a greater proportion of lithogenic material (e.g., clays) and lower productivity. Therefore, X-radiograph gray scale constitutes an ultrahigh-resolution proxy record for surface productivity. A visual comparison of X-radiograph gray scale with XRF Fe and Ti data shows an excellent covariance with sediment density (Figures 6a, 6f, and 6g). Since in continental margin sediments, Fe and Ti are found predominately in the denser lithogenic fraction [*Calvert and Pedersen*, 1993], this result further supports our interpretation of X-radiograph gray scale as a proxy for surface productivity in this setting.

[11] We also use centimeter-scale measured N (wt%) and XRF Si/Ti ratios (submillimeter scale) as more conventional proxies of organic and siliceous (biogenic opal) productivity respectively. Depth profiles of opaline silica content (measured by chemical extraction in 2M Na_2CO_3 method [*Mortlock and Froelich*, 1989]) and ICP-AES Si/Ti ratio in core ODP1228D were found to be

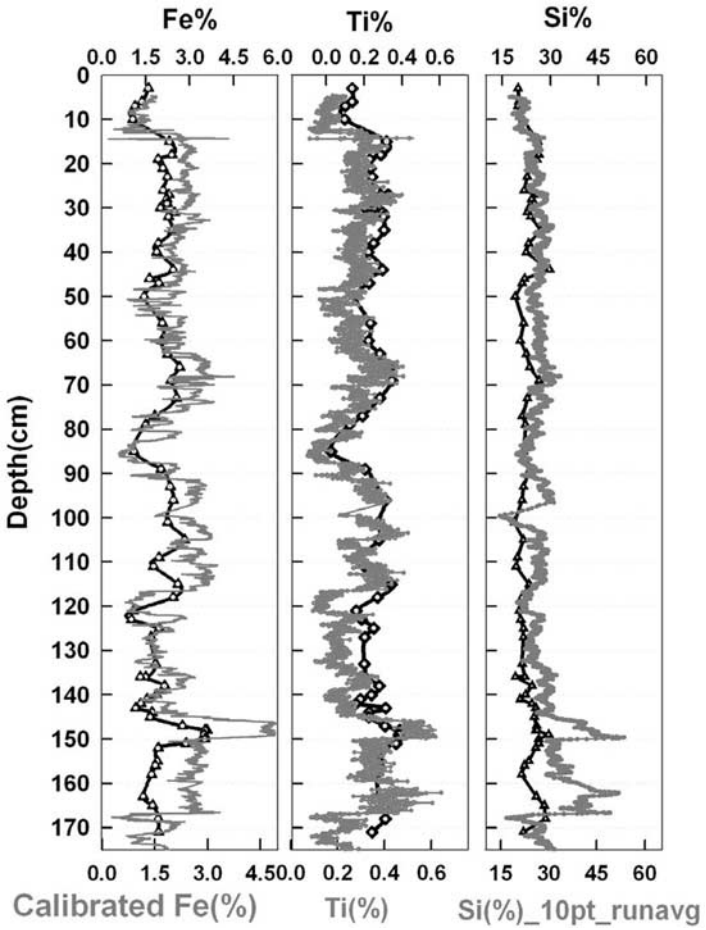

Figure 4. Comparison of Fe, Ti, and Si contents, measured by scanning XRF (at depth resolution of 0.04 cm; shown in gray) with ICP-AES (at cm resolution; shown as black triangles) for core W40.

statistically well correlated (data not shown). This supports the reliability of ultrahigh-resolution Si/Ti ratios as a proxy for siliceous productivity in the study region. As expected, lighter X-radiograph gray scale also correlates with N (wt%) and Si/Ti ratio (Figures 6a, 6b, and 6d). Ultrahigh-resolution Si/Ti ratios exhibit very high amplitude and high frequency variability and are, therefore, plotted on a log scale (Figure 6d). Fluvial, lacustrine, and marine sediments have been found to contain significant concentrations of organohalogens which cannot be explained by known anthropogenic halogen compounds [*Müller et al.*, 2004], indicating sedimentary Br could be used as indicator of organic productivity in coastal organic-rich environments such as Peru margin. Ultrahigh-resolution Br data when normalized with Ti also show the high-amplitude and high-frequency variability seen in the Si/Ti depth profile.

[12] Recent paleoreconstructions from the Peru margin used lithic sediment fraction (measured by reflectance spectra) as a proxy for continental lithogenic material supplied to shelf sediments during strong El Niño-related precipitation events [*Rein et al.*, 2004, 2005]. However, the concentration of any component in the sediment, biogenic or lithogenic is also a function of dilution by other components. We take an alternative view that lithogenic material in this highly productive region acts mainly as a diluent for the biogenic component of the sediments. Variability in sedimentary concentrations of lithogenic tags such as Fe and Ti arises from the production and accumulation of biogenic opal in the sediments and to a lesser degree OM. Ultrahigh-resolution Fe and Ti data may thus be used as negative indices of surface productivity assuming that changes in Fe and Ti contents due to past land runoff variability are small as compared to net dilution effect caused be relatively larger

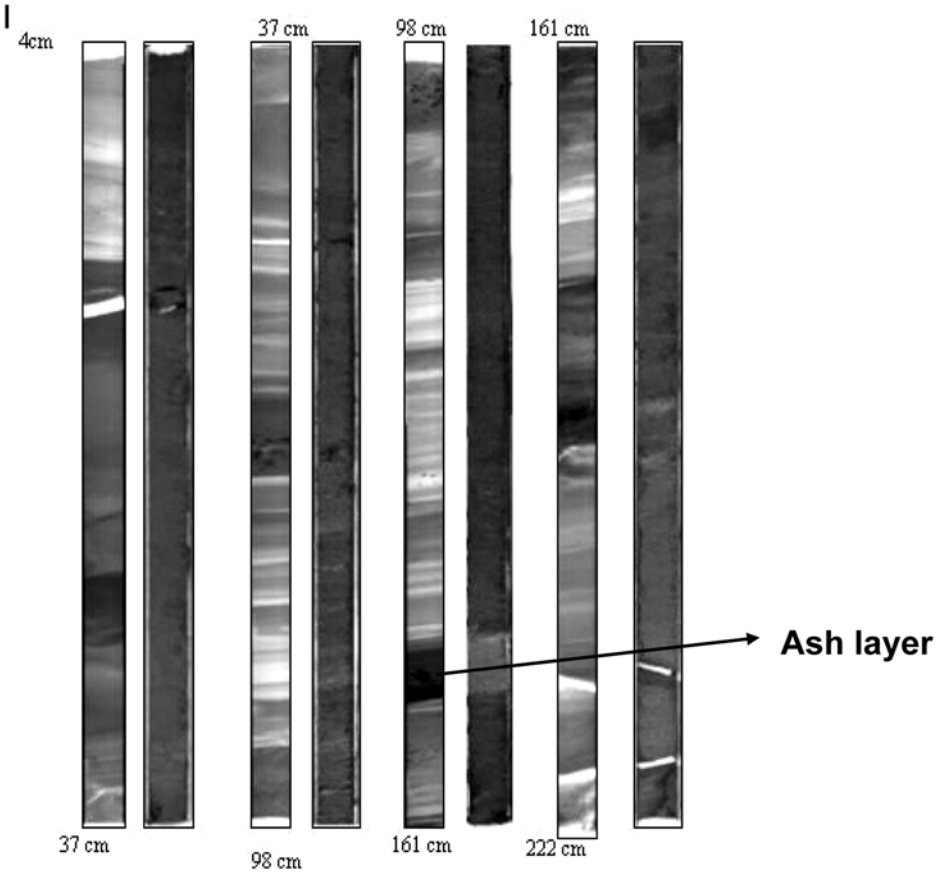

Figure 5. X-radiographs and optical images of core W7706-40. X-radiographs show presence of laminations throughout in the form of density variations. Lighter portions have relatively higher proportions of surface-produced biogenic components as compared to denser (darker) lithogenic material.

productivity changes. In addition, surface productivity and coastal runoff are both inversely related in modern climatic conditions off Peru, i.e., during normal/La Nina conditions (ENSO) when surface productivity off Peru is high (lower), contribution of land runoff is very small (higher) due to prevailing arid (wet) conditions inland of the Peru coast. Therefore, modern climatic conditions off Peru also support the view that Fe and Ti are negative indices of surface productivity at the core site. Ti is better for this purpose than Fe, which is subject to early diagentic (redox) effects. However, depth profiles of both Fe and Ti are strikingly similar during the entire depositional history of core W40 (Figure 6) as previously observed in the Cariaco basin [*Haug et al.*, 2001]. In the next section, we also use the depth profile of sedimentary $\delta^{15}N$ as a proxy for subsurface denitrification in the Peru margin to further evaluate the validity of our interpretation.

4.2. Sedimentary $\delta^{15}N$ as Index of Subsurface Denitrification

[13] The Arabian Sea (off the Oman margin), ETNP (off the western Mexican margin) and ETSP (off Peru and Chilean margin) are the major oceanic regions with suboxic intermediate waters produced by poor ventilation and high downward flux of OM. Water column denitrification in the subsurface waters of these regions (OMZs) produces extensive isotopic fractionation ($\varepsilon \sim 20$ to 30‰), leaving the remaining NO_3^- pool enriched in ^{15}N [*Liu and Kaplan*, 1989; *Brandes et al.*, 1998], which subsequently is transferred by upwelling into the phytoplankton community and eventually, sedimentary OM. Under conditions of complete surface nutrient utilization, sinking OM ultimately leaves this enriched ^{15}N signature in underlying sediments. Combined water column NO_3^-, sediment trap and surface sediment $\delta^{15}N$ data confirm isotopic balance between influx of NO_3^- into the

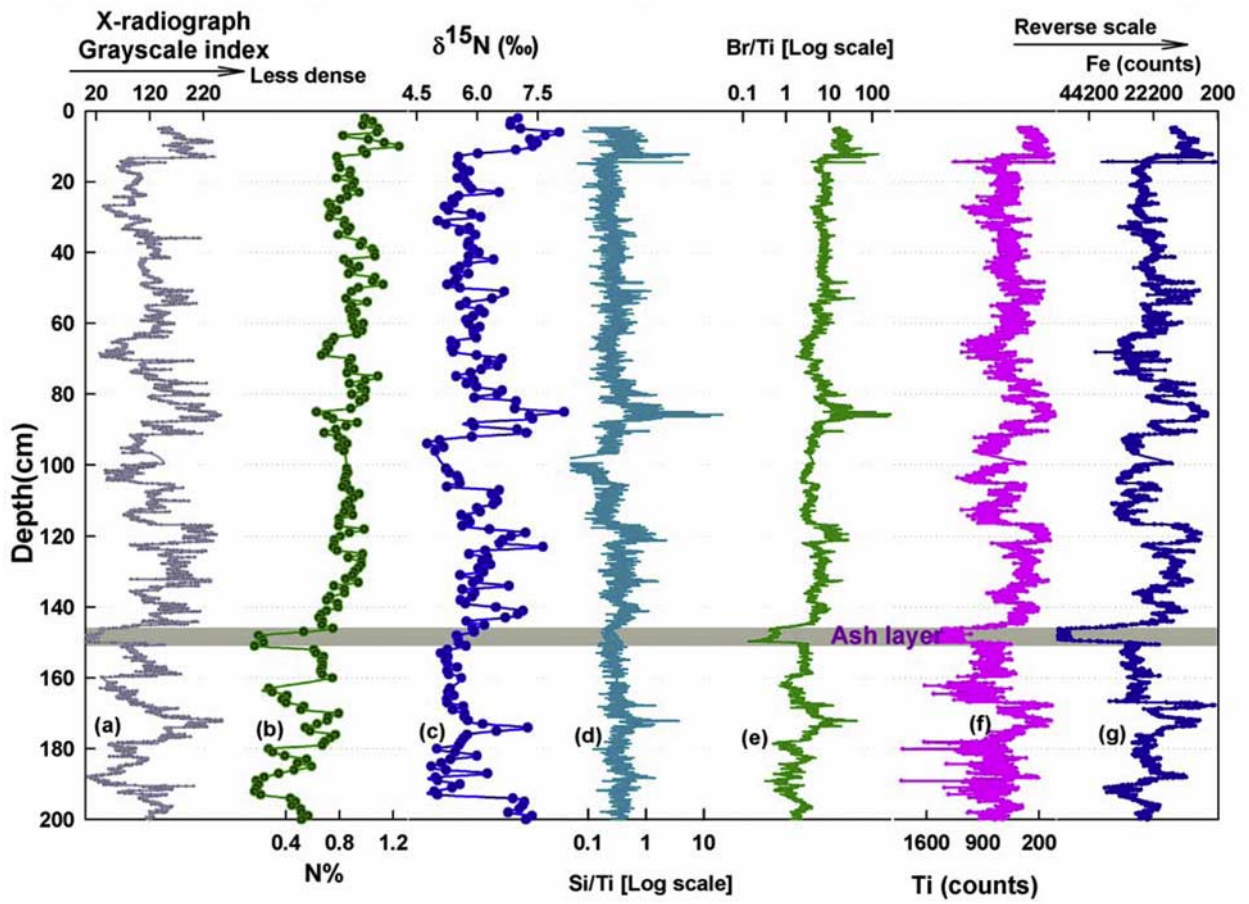

Figure 6. Centennial to subdecadally resolved multiproxy data of core W40. (a, b, d, and e) Surface productivity indices (N%, Si/Ti, and Br/Ti ratios) correlate with lighter gray scale together with bulk δ^{15}N. (a, f, and g) Ti and Fe are major components of denser lithogenic material and thus anticorrelate with productivity indices. Horizontal gray bar shows the presence of an ash layer.

euphotic zone and loss from sinking particles [*Schäfer and Ittekkot*, 1993; *Altabet et al.*, 1999]. Thus, sedimentary δ^{15}N has been successfully used as a reliable tool to track past changes in water column denitrification. Denitrification in turn was found to be strongly coupled with global climate changes during the late-Quaternary as mediated by changes in upwelling-stimulated productivity and/or ventilation of subsurface waters [*Altabet et al.*, 1995, 1999, 2002; *Ganeshram et al.*, 1995, 2000]. Fe limitation of phytoplankton production in the oceanic high-nutrient low-chlorophyll (HNLC) region off Peru could result in partial utilization of nutrients thereby influencing the δ^{15}N of sinking OM. However, modern upwelled waters on the central Peru margin have been found to be Fe-rich due to contact with reducing sediments [*Bruland et al.*, 2005]. In fact, in the core of the Peru margin denitrification zone (~15°S), both water column water NO_3^- and sedimentary δ^{15}N data show large isotopic enrichment (up to 10–11‰ [*Liu*, 1979]). This δ^{15}N signal is thus faithfully transferred to Peru margin sediments as is the case for the Arabian Sea and ETNP [*Altabet*, 2005] and should reflect the denitrification history of subsurface waters off Peru.

[14] The δ^{15}N depth profile of core W40 shows a striking covariance with X-radiograph gray scale (Figures 6a and 6c). This covariance of δ^{15}N with surface productivity index is of vital significance as it first rules out the possibility of Fe limitation influencing sedimentary δ^{15}N in the study region. Otherwise during lower surface productivity, Fe limitation would lead to higher δ^{15}N due to complete utilization of a reduced NO_3- flux to surface waters. Second, good covariance between δ^{15}N and gray scale index (surface productivity) shows that variations in Peru margin denitrification were very likely controlled by surface productivity during the last ~2300 years (Figure 7). Though the excellent

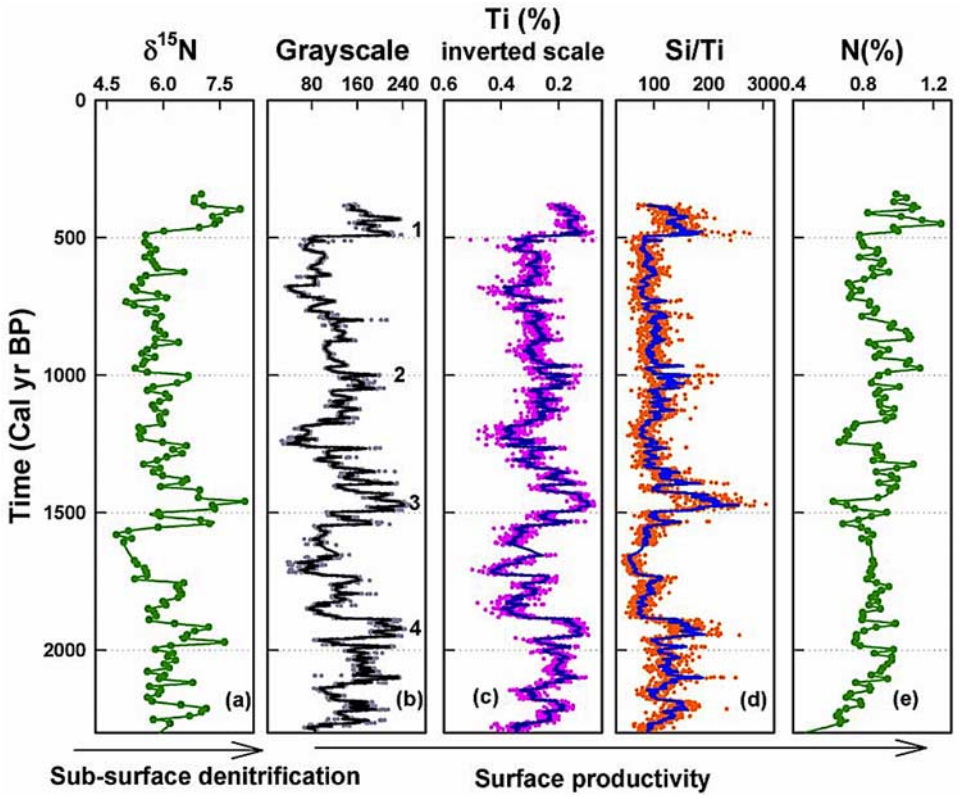

Figure 7. Subsurface denitrification and surface productivity variations off the Peru during the last ~2300 years. Ten point moving averages of ultrahigh-resolution gray scale, Ti, and Si/Ti data are shown as solid lines.

covariance found between gray scale and δ^{15}N does not unequivocally rule out the possibility of dilution by terrigenous material, it certainly suggests productivity variations were dominant enough to induce changes in subsurface suboxic conditions; therefore, we find it less likely that there were large variations in delivery of clays as compared to diatom productivity on this arid margin.

4.3. Ultrahigh-Resolution Variability in Peru Margin Productivity

[15] The age-depth model for core W40 indicates linear sedimentation (r^2 = 0.98) for last ~2.3 ka B.P. before which sedimentation rate was significantly reduced (Figure 1 inset). Using our established proxies, i.e., gray scale, Si/Ti ratios, N content and δ^{15}N, we reconstruct surface productivity and subsurface denitrification changes of the Peru margin for the best resolved part of this record, the last ~300 to 2300 years (Figure 7). Owing to presence of obvious cracks due to drying of sediment core top (of W40), the initial 0 to 4 cm XRF data is not continuous, and therefore omitted from the depth profiles shown. Most of the productivity proxies show a series of correlated peaks and valleys of millennial to decadal scale. N (wt%) shows the weakest signal, δ^{15}N is well correlated with the proxies for biogenic opal deposition. Figures 7b, 7c, and 7d clearly show that there are at least 4 major events at ~500, 1000, 1450 and ~1800 years B.P. when surface productivity (coupled with subsurface denitrification) intensified and persisted for ~50 years. Our proxy indicators for the biogeochemical system off Peru show the dominance of centennial-scale variability upon which lower-amplitude, higher-frequency variability is superimposed.

[16] This record is remarkable in showing the late Holocene Peru margin to be characterized by persistent moderate productivity and less intense denitrification that is punctuated at centennial scale by relatively shorter-duration periods of high production and intense denitrification. These events are likely analogous to modern observations of decadal-scale "regime shifts" not only along the Peru margin but also coincidently across the entire Pacific [*Chavez et al.*, 2003]. A persistent El Nino-like interval from the 1970s to 1990s was marked by depressed thermocline depth along the western South America coast [*Pizzaro and Montecinos*,

2004] and reduced Equatorial Tropical Pacific flow and upwelling [*McPhaden and Zhang*, 2004]. Though its ultimate forcing is not clear, the tropical Pacific is clearly capable of longer-term restructuring of its hydrography and flow fields to produce ENSO-like oscillations at longer periods. Our results demonstrate even higher amplitude variability at the centennial-scale that has not, as of yet, been observed during the modern instrumental period. It should be of general concern that modern conditions on the Peru margin may be more representative of the shorter-lived, higher productivity intervals observed in core W40. Our results indicate a reasonable likelihood in the near future of a natural switch back to the lower productivity (and less intense denitrification) more typical of the last two millennia.

4.4. Spectral Analysis of Paleoproductivity Proxies

[17] Spectral analysis was used to more rigorously characterize periodicities in Peru margin productivity. As significant "noise" could be expected with ultrahigh-resolution gray scale and Ti data; 4 point binning (block averaging) of proxy data sets were carried out and splined to yield a temporal resolution of ~2 years, still sufficient for detection of frequencies from the ENSO (subdecadal) to centennial range. Spectral analyses of the proxy data spanning a period from ~300a to 2.3 ka B.P. were carried out using the multitaper method [*Mann and Lees*, 1996] (http://www.atmos.ucla.edu/tcd/ssa/). Results of spectral analyses of gray scale index and Ti data of core W40 show multiple significant cycles of ~250, 154, 83, ~56–38, ~22–24, ~11–9.4, ~7.4–5.7 years (Figure 8). While cycles of ~83, 22–24 and ~11–9.4 years may be of solar origin, periodicities of ~7.4–5.8 years fall within the ENSO range (3 to 7 years). Presence of other multidecadal periodicities might be attributed to several decadal-scale ocean-atmospheric feedback processes controlling surface productivity and mutual interactions among them giving rise to other coupled modes such as PDOs.

5. Plausible Solar Forcing of Peru Margin Productivity

[18] Decadal to centennial-scale variability in Peru productivity is likely manifest through the mean latitudinal position of ITCZ at the extremes of its seasonal oscillation. The ITCZ is a circum-global atmospheric belt of upward convection and rainfall marking the confluence of northern and southern trade winds. A more northerly (southerly) position likely leads to higher (lower) surface productivity off Peru by analogy to normal/La Niña (El Niño) conditions probably through increase in upwelling favorable winds as well as the depth of oxyclines and nutriclines along the Peru coast. The global extent of ITCZ climatically links regions otherwise remote from each other (e.g., Peru and South Asia). Sensitivity of major climate phenomena such as the Indian monsoon and ENSO to ITCZ position has been demonstrated in both paleoclimatic records as well as model simulations [*Fleitmann et al.*, 2003; *Clement et al.*, 1999]. A more northerly position of ITCZ during N. Hemisphere summer favors stronger convective cloud development and higher monsoonal precipitation over Arabia and India [*Fleitmann et al.*, 2003; *Gupta et al.*, 2003] as well as higher precipitation in northern S. America (Venezuela) [*Haug et al.*, 2001]. On the other hand, a southerly position of ITCZ coincides with ENSO conditions in South Pacific, i.e., lower surface productivity off Peru and above average rainfall on normally arid continental parts of Ecuador and Peru [*Moy et al.*, 2002]. At greater than millennial timescales, changes in mean latitudinal position of ITCZ are known to be strongly influenced by the seasonal distribution of solar insolation as governed by orbital forcing [*Clement et al.*, 1999; *Haug et al.*, 2001; *Wang et al.*, 2005]. As an exaggerated seasonal southward migration of ITCZ at the beginning of austral summer is known to be an initiating event for modern El Niño [*Philander*, 1983], solar (irradiance) variability influencing overall background ENSO state of the Peru margin specifically through ITCZ position is anticipated.

[19] Satellite-based yearly total solar irradiance (TSI) data have only been available for the last two decades, but reconstructed TSI records dating to 1610 C.E. were first made on the basis of parameterization of sunspot darkening and facular brightening [*Lean et al.*, 1995]. Reconstructed TSI was subsequently extended back to 843 C.E. on the basis of a quantitative estimate of common variations in the production rates of ^{14}C and ^{10}Be cosmogenic radionuclides [*Bard et al.*, 2000]. Most recently, dendrochronologically dated radiocarbon content, was used to reconstruct sunspot number (positively correlated with small variations in solar irradiance) for the past ~11,000 years [*Solanki et al.*, 2004]. The influence of past solar forcing on global climate can thus be assessed by a direct comparison of temporal variability in TSI/sunspot numbers with contemporaneous, temporally well-

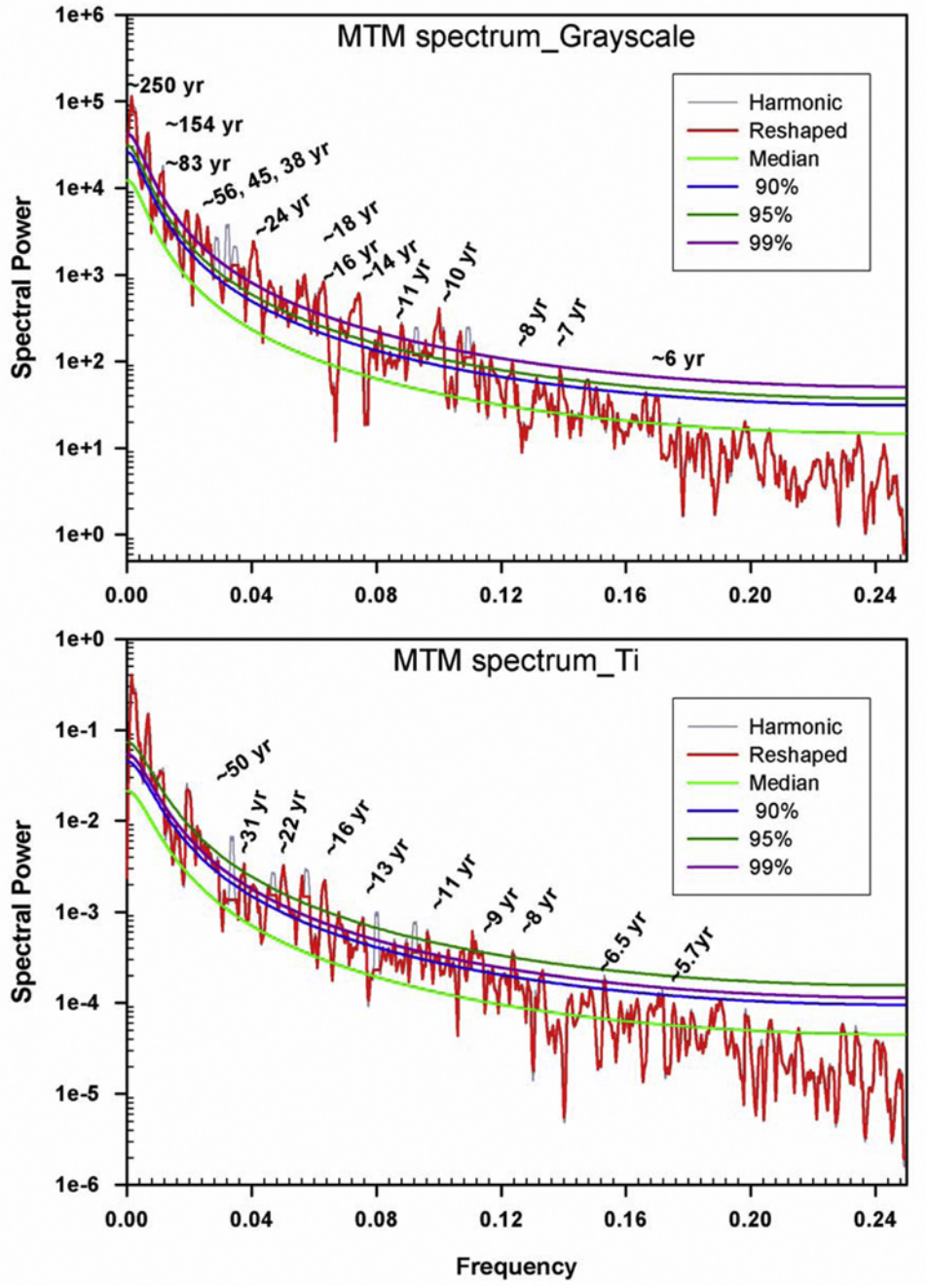

Figure 8. Spectral analysis of gray scale and Ti data using the multitaper method [*Mann and Lees*, 1996]. Ultrahigh-resolution gray scale and calibrated Ti data were first binned (block averaged) to 4 points and then splined to yield to a temporal resolution ~2.0 years. Significance lines indicate 90, 95, and 99% confidence limits.

resolved, paleoclimatic records. Well-dated and temporally well-resolved paleoreconstructions from "climatically sensitive" locations such as the Peru margin are accordingly likely to provide clues to the "physical link" connecting small solar irradiance variability and Earth's climate.

[20] Peru productivity and past sunspot number (SN) (Figures 9a and 9b) show visual similarity during the last ~2300 years. Despite having different temporal resolutions and associated age uncertainties in both time series, Peru productivity based on X-radiograph gray scale for core W40 shows a poor, but still significant correlation ($r = 0.41$; $p > 0.01$) with SN (data not shown) especially when no chronological adjustment was made in order to improve the positive correlation.

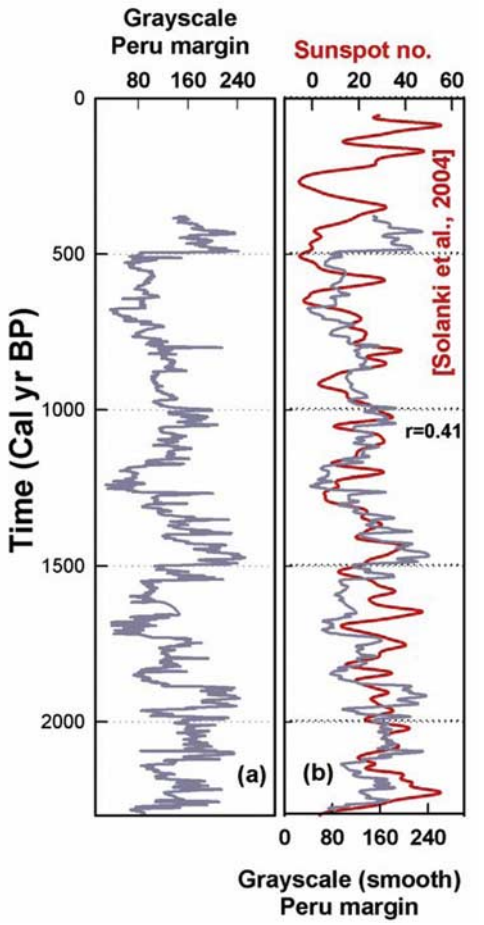

Figure 9. (a) Peru margin productivity shows significant covariance with (b) reconstructed solar variability on decadal to centennial scale during the last ~2300 years.

Similar observations have been made previously for analogous low-latitude regions. For instance, Indian summer monsoon intensity together with surface productivity of northeastern Arabian Sea was strongly correlated with decadal to centennial-scale variations in TSI during the last millennium [*Agnihotri et al.*, 2002; *Gupta et al.*, 2003; *Agnihotri and Dutta*, 2003].

[21] Modern data showing good correlations between southern oscillation index (SOI) and sea surface temperature gradient across the Arabian Sea (ΔSST) as well as the presence of solar cycles in the SOI index have indicated plausible coupling between intensity of Indian monsoon and ENSO, through solar variability [*Higginson et al.*, 2004]. Strong El Niño events coincide precisely with minimum solar irradiance during the solar cycle in the modern data [*Higginson et al.*, 2004]. While solar irradiance variability could be a triggering mechanism on decadal to centennial-scale climate change [*Poore et al.*, 2004], its actual manifestation in regional climate variables require amplifying mechanism(s) due to the low absolute amplitude in TSI variations. Various physical mechanisms have been proposed to produce this amplification, including alteration of the atmospheric circulation pattern as a result of changes in solar ultraviolet radiation during the solar cycle [*Shindell et al.*, 1999; *Haigh*, 2001]. The exact physical mechanism involved in the observed coupling between solar irradiance changes at the top of the atmosphere and upwelling stimulated surface productivity in coastal waters off Peru (this study) and northeastern Arabian Sea [*Agnihotri et al.*, 2002] is still not yet clear. However, sensitivity of the mean latitudinal position of ITCZ to solar irradiance changes may be one pathway [*Agnihotri et al.*, 2002; *Agnihotri and Dutta*, 2003; *Higginson et al.*, 2004]. Stratospheric modulation of upwelling in the equatorial troposphere, which produces a north-south seesaw of convective activity during seasonal migration of ITCZ from northern to southern hemisphere, may be a more acceptable pathway [*Kodera*, 2004]. Coral records have also been used to infer paleo-ENSO activity in the tropical Pacific for the last millennium [*Cobb et al.*, 2003]. A direct comparison of inferred Peru margin productivity and Coral isotopic data for the contemporaneous period is not attempted due to patchiness involved in later record, however, our study appears to be consistent with the major outcome of the *Cobb et al.* [2003], i.e., most intense ENSO activity occurred during mid-17th century, a period of lowest solar activity (Little Ice Age) during the last millennium. Similarly, we also note apparent similarity between inferred temperature changes in Huascarán ice core data [*Thompson et al.*, 1995] with sunspot activity on centennial timescales during last two millennia, thus corroborating a major outcome of our study, i.e., decadal- to centennial-scale solar variability appears to be a major underlying forcing mechanism governing climate of the last two millennia.

[22] We have attempted to understand inferred Peru margin productivity in light of solar intrinsic variability (changes in solar irradiance or sunspot activity) though it is also known that volcanic eruptions forced abrupt climate changes in recent millennia [*Crowley*, 2000; *Shindell et al.*, 2003]. Where solar intrinsic variability (solar irradiance changes) is likely to introduce quasiperiodic variability in the Earth's climate, short-duration volca-

nic eruptions inject aerosols (mainly SO_4^-) into the atmosphere producing short-term and singular events. Though best agreement with historical and proxy data is obtained using both solar and volcanic forcings, general circulation models results [*Shindell et al.*, 2003] suggest that, long-term regional changes during the preindustrial period appear to have been dominated by solar forcing. Due to opposing dynamical and radiative effects, the long-term (decadal-scale) regional response to volcanic forcing is not significant as compared to unforced variability for either seasonal or the annual average. In contrast, the long-term regional response to solar variability greatly exceeds unforced variability as the dynamical and radiative effects reinforce each other and produces climate anomalies similar to the Little Ice age.

6. Conclusions and Implications

[23] On the basis of a multiproxy data of sedimentary record from the Peru margin, we reconstruct subdecadally resolved paleoceanographic history of the Peru margin for the last ~2300 years. During this period, surface productivity is found to be intimately coupled with subsurface denitrification intensity as measured by sediment $\delta^{15}N$ demonstrating the validity of our interpretive framework. Peru margin productivity, known to be extremely sensitive to modern ENSO phenomena, shows strong decadal- to centennial-scale variability during the last two millennia which may have a significant forcing component from solar variability as observed in other contemporaneous studies [*Yu and Ito*, 1999; *Hu et al.*, 2003; *Weber et al.*, 2004; *Mangini et al.*, 2005]. These events likely correspond to large-scale restructuring of tropical Pacific hydrography and circulation as observed at decadal scale in the modern period but amplified at the centennial scale. Periods of high productivity and more intense denitrification were interspersed by periods of reduced productivity and denitrification. High productivity observed during the recent instrumental period may thus not persistently characterize the Peru margin into the near future. Additional well-dated ultrahigh-resolution paleoreconstructions from climatically sensitive marine regions such as the Peru margin are recommended for better understanding of the underlying forcing mechanism(s) governing climate of the recent past.

Acknowledgments

[24] This research is sponsored by the U.S. National Science Foundation (NSF grants 0318371 and 0353311). We acknowledge the technical assistance provided by P. Feng and R. Singh and Matt Higginson for supplying ^{14}C dates. We thank the core curators of the ODP and OSU core repositories for providing sediment samples. We also thank K. Dutta (IOP, Bhubneshwar) for help with MTM spectral analyses. Jeff Donnelly (WHOI) kindly provided access to the XRF facility. This is UMD SMAST Contribution Series 08-0401, School for Marine Science and Technology, University of Massachusetts Dartmouth.

References

Agnihotri, R., and K. Dutta (2003), Centennial scale variations in monsoonal rainfall (Indian, east equatorial and Chinese monsoons): Manifestations of solar variability, *Curr. Sci.*, *85*, 459–463.

Agnihotri, R., K. Dutta, R. Bhushan, and B. L. K. Somayajulu (2002), Evidence for solar forcing on the Indian monsoon during the last millennium, *Earth Planet. Sci. Lett.*, *198*, 521–527, doi:10.1016/S0012-821X(02)00530-7.

Altabet, M. A. (2005), Isotopic tracers of the marine nitrogen cycle, in *Marine Organic Matter: Chemical and Biological Markers, Handb. Environ. Chem.*, vol. 2, edited by J. Volkman, pp. 251–293, Springer, New York, doi:10.1007/698_2_008.

Altabet, M. A., R. François, D. W. Murray, and W. L. Prell (1995), Climate-related variations in denitrification in the Arabian Sea from sediment $^{15}N/^{14}N$ ratios, *Nature*, *373*, 506–509, doi:10.1038/373506a0.

Altabet, M. A., D. W. Murray, and W. L. Prell (1999), Climatically linked oscillations in Arabian Sea denitrification over the past 1 m.y.: Implications for the marine N cycle, *Paleoceanography*, *14*, 732–743, doi:10.1029/1999PA900035.

Altabet, M. A., M. J. Higginson, and D. W. Murray (2002), The effect of millennial-scale changes in Arabian Sea denitrification on atmospheric CO_2, *Nature*, *415*, 159–162, doi:10.1038/415159a.

Arntz, W., and E. Fahrbach (1991), *El Niño-Klimaexperiment der Nature*, 263 pp., Springer, New York.

Bard, E., G. Raisbeck, F. Yiou, and J. Jouzel (2000), Solar irradiance during the last 1200 years based on cosmogenic nuclides, *Tellus, Ser. B*, *52*, 985–992, doi:10.1034/j.1600-0889.2000.d01-7.x.

Bond, G. B., B. Kromer, J. Beer, R. Muscheler, M. N. Evans, W. Showers, S. Hoffmann, R. Lotti-Bond, I. Hajdas, and G. Bonani (2001), Persistent solar influence on North Atlantic climate during the Holocene, *Science*, *294*, 2130–2136, doi:10.1126/science.1065680.

Brandes, J. A., A. H. Devol, T. Yoshinari, D. A. Jayakumar, and S. W. A. Naqvi (1998), Isotopic composition of nitrate in the central Arabian Sea and eastern tropical North Pacific: A tracer for mixing and nitrogen cycles, *Limnol. Oceanogr.*, *43*, 1680–1689.

Bruland, K. W., E. L. Rue, G. J. Smith, and G. R. DiTullio (2005), Iron, macronutrients and diatom blooms in the Peru upwelling regime: Brown and blue waters of Peru, *Mar. Chem.*, *93*, 81–103, doi:10.1016/j.marchem.2004.06.011.

Calvert, S. E., and T. F. Pedersen (1993), Geochemistry of oxic and anoxic sediments: Implications for the geological record, *Mar. Geol.*, *113*, 67–88, doi:10.1016/0025-3227(93)90150-T.

Cane, M., and A. C. Clement (1999), A role for tropical Pacific coupled ocean atmosphere system on Milankowitch and millennial time scales: Part 2. Global impacts, in *Mechanisms of Global Climate Change at Millennial Time Scales*, *Geophys.*

Monogr. Ser., vol. 12, edited by P. U. Clark, R. S. Webb, and L. D. Keigwin, pp. 373–383, AGU, Washington, D. C.

Chavez, F. P., et al. (2003), From anchovies to sardines and back: Multidecadal change in the Pacific Ocean, *Science*, *299*, 217–221, doi:10.1126/science.1075880.

Clement, A. C., R. Seager, and M. A. Cane (1999), Orbital controls on the El Niño/Southern Oscillation and the tropical climate, *Paleoceanography*, *14*, 441–456, doi:10.1029/1999PA900013.

Cobb, K. M., C. D. Charles, H. Cheng, and R. L. Edwards (2003), El Niño/Southern Oscillation and tropical Pacific climate during the last millennium, *Nature*, *424*, 271–276.

Codispoti, L. A., et al. (1986), High nitrite levels off Northern Peru: A signal of instability in the marine denitrification rate, *Science*, *233*, 1200–1202, doi:10.1126/science.233.4769.1200.

Croudace, I. W., A. Rindby, and R. G. Rothwell (2006), ITRAX: Description and evaluation of a new sediment core scanner, in New Ways of Looking at Sediment Cores and Core Data, edited by R. G. Rothwell, *Geol. Soc. Spec. Publ.*, *267*, 51–63.

Crowley, T. J. (2000), Causes of climate change over the past 1000 years, *Science*, *289*, 270–277, doi:10.1126/science.289.5477.270.

Fleitmann, D., S. J. Burns, M. Mudelsee, U. Neff, J. Kramers, A. Mangini, and A. Matter (2003), Holocene forcing of the Indian monsoon recorded in a stalagmite from southern Oman, *Science*, *300*, 1737–1739, doi:10.1126/science.1083130.

Ganeshram, R. S., T. F. Pedersen, S. E. Calvert, and J. M. Murray (1995), Large changes in oceanic inventories from glacial to interglacial periods, *Nature*, *376*, 755–758, doi:10.1038/376755a0.

Ganeshram, R. S., T. F. Pedersen, S. E. Calvert, and G. W. McNeil (2000), Glacial-interglacial variability in denitrification in the world's oceans: Causes and consequences, *Paleoceanography*, *15*, 361–376, doi:10.1029/1999PA000422.

Gupta, A. K., D. M. Anderson, and J. T. Overpeck (2003), Abrupt changes in the Asian southwest monsoon during the Holocene and their links to the North Atlantic Ocean, *Nature*, *421*, 354–357, doi:10.1038/nature01340.

Haigh, J. D. (2001), Climate variability and the influence of the Sun, *Science*, *294*, 2109–2111, doi:10.1126/science.1067013.

Haug, G. H., A. K. Hughen, D. M. Sigman, L. C. Peterson, and U. Röhl (2001), Southward migration of the Intertropical Convergence Zone through the Holocene, *Science*, *293*, 1304–1308, doi:10.1126/science.1059725.

Higginson, M. J., and M. A. Altabet (2004a), Initial test of the silicic acid leakage hypothesis using sedimentary biomarkers, *Geophys. Res. Lett.*, *31*, L18303, doi:10.1029/2004GL020511.

Higginson, M. J., M. A. Altabet, L. Wincze, T. D. Herbert, and D. W. Murray (2004b), A solar (irradiance) trigger for millennial-scale abrupt changes in the southwest monsoon, *Paleoceanography*, *19*, PA3015, doi:10.1029/2004PA001031.

Hu, F. S., D. Kaufman, S. Yoneji, D. Nelson, A. Shemesh, Y. Huang, J. Tian, G. Bond, B. Clegg, and T. Brown (2003), Cyclic variation and solar forcing of Holocene climate in the Alaskan subarctic, *Science*, *301*, 1890–1893, doi:10.1126/science.1088568.

Kodera, K. (2004), Solar influence on the Indian Ocean Monsoon through dynamical processes, *Geophys. Res. Lett.*, *31*, L24209, doi:10.1029/2004GL020928.

Kudrass, H. R. (Ed.) (2000), Cruise Report SO147 Peru upwelling: Valparaiso–Callao, 29.05–03.07.2000, BRG Hanover, Hanover, Germany.

Lean, J., J. Beer, and R. Bradley (1995), Reconstruction of solar irradiance since 1610: Implications for climate change, *Geophys. Res. Lett.*, *22*(23), 3195–3198, doi:10.1029/95GL03093.

Linsley, B. K., L. Ren, R. B. Dunbar, and S. S. Howe (2000), El Niño Southern Oscillation (ENSO) and decadal-scale climate variability at 10°N in the eastern Pacific from 1893 to 1994: A coral-based reconstruction from Clipperton Atoll, *Paleoceanography*, *15*(3), 322–335, doi:10.1029/1999PA000428.

Liu, K. K. (1979), Geochemistry of inorganic nitrogen compounds in two marine environments: The Santa Barbara basin and the ocean off Peru, doctoral thesis, Univ. of California, Los Angeles, Los Angeles.

Liu, K. K., and I. R. Kaplan (1989), The eastern tropical Pacific as a source of ^{15}N enriched nitrate in seawater off southern California, *Limnol. Oceanogr.*, *5*, 820–830.

Mangini, A., C. Spotl, and P. Verdes (2005), Reconstruction of temperature in the Central Alps during the past 2000 yr from a $\delta^{18}O$ stalagmite record, *Earth Planet. Sci. Lett.*, *235*, 741–751, doi:10.1016/j.epsl.2005.05.010.

Mann, M. E., and J. M. Lees (1996), Robust estimation of background noise and signal detection in climatic time series, *Clim. Change*, *33*, 409–445, doi:10.1007/BF00142586.

McPhaden, M. J., and D. Zhang (2004), Pacific Ocean circulation rebounds, *Geophys. Res. Lett.*, *31*, L18301, doi:10.1029/2004GL020727.

Mortlock, R. A., and P. N. Froelich (1989), A simple method for the rapid determination of biogenic opal in pelagic marine sediments, *Deep Sea Res., Part A*, *36*, 1415–1426, doi:10.1016/0198-0149(89)90092-7.

Moy, C. M., G. O. Seltzer, D. T. Rodbell, and D. M. Anderson (2002), Variability of El Niño/Southern Oscillation activity at millennial timescales during the Holocene epoch, *Nature*, *420*, 162–165, doi:10.1038/nature01194.

Müller, G., G. Nkusi, and H. F. Schöler (2004), Natural organohalogens in sediments, *J. Prakt. Chem. Chem. Ztg.*, *338*, 23–29.

Philander, S. G. H. (1983), El Nino Southern Oscillation phenomena, *Nature*, *302*, 295–301, doi:10.1038/302295a0.

Pizarro, O., and A. Montecinos (2004), Interdecadal variability of the thermocline along the west coast of South America, *Geophys. Res. Lett.*, *31*, L20307, doi:10.1029/2004GL020998.

Poore, R. Z., T. M. Quinn, and S. Verado (2004), Century-scale movement of the Atlantic Intertropical Convergence Zone linked to solar variability, *Geophys. Res. Lett.*, *31*, L12214, doi:10.1029/2004GL019940.

Reimers, C., and E. Suess (1983), Spatial and temporal patterns of organic matter accumulation on the Peru continental margin, in *Coastal Upwelling, Its Sedimentary Record: Part B, Sedimentary Records of Ancient Coastal Upwelling*, edited by J. Thiede and E. Suess, pp.311–345, Plenum, New York.

Rein, B., A. Lückge, and F. Sirocko (2004), A major Holocene ENSO anomaly during the Medieval period, *Geophys. Res. Lett.*, *31*, L17211, doi:10.1029/2004GL020161.

Rein, B., A. Lückge, L. Reinhardt, F. Sirocko, A. Wolf, and W.-C. Dullo (2005), El Niño variability off Peru during the last 20,000 years, *Paleoceanography*, *20*, PA4003, doi:10.1029/2004PA001099.

Schäfer, P., and V. Ittekkot (1993), Seasonal variability of $\delta^{15}N$ in settling particles in the Arabian Sea and its paleogeochemical significance, *Naturwissenschaften*, *80*, 511–513, doi:10.1007/BF01140806.

Shindell, D., D. Rind, N. Balachandran, J. Lean, and P. Lonergn (1999), Solar cycle variability, ozone, and climate, *Science*, *284*, 305–308, doi:10.1126/science.284.5412.305.

Shindell, D. T., G. A. Schmidt, R. L. Miller, and M. E. Mann (2003), Volcanic and solar forcing of climate change during the preindustrial era, *J. Clim.*, *16*, 4094–4107, doi:10.1175/1520-0442(2003)016<4094:VASFOC>2.0.CO;2.

Solanki, S. K., I. G. Usoskin, B. Kromer, M. Schüssler, and J. Beer (2004), Unusual activity of the Sun during recent decades compared to the previous 11,000 years, *Nature*, *431*, 1084–1087, doi:10.1038/nature02995.

Thompson, L. G., E. M. Thompson, M. E. Davis, P.-N. Lin, K. A. Henderson, J. Cole-Dai, J. F. Bolzan, and K.-b. Liu (1995), Late glacial stage and Holocene tropical ice core records from Huascarán, Peru, *Science*, *269*, 46–50, doi:10.1126/science.269.5220.46.

Wang, Y., H. Cheng, R. L. Edwards, Y. He, X. Kong, J. An, M. J. Kelly, C. A. Dykoski, and X. Li (2005), The Holocene Asian Monsoon: Links to solar changes and north Atlantic climate, *Science*, *308*, 854–857, doi:10.1126/science.1106296.

Weber, S. L., T. J. Crowley, and G. V. Schrier (2004), Solar irradiance forcing of centennial climate variability during the Holocene, *Clim. Dyn.*, *22*, 539–553, doi:10.1007/s00382-004-0396-y.

Yu, Z., and E. Ito (1999), Possible solar forcing of century scale drought frequency in the northern Great Plains, *Geology*, *27*, 263–266, doi:10.1130/0091-7613(1999)027<0263:PSFOCS>2.3.CO;2.